Int J Adv Struct Eng (2016) 8:379–389
DOI 10.1007/s40091-016-0139-4

ORIGINAL RESEARCH

Wind-induced vibrations of structures using design spectra

P. Martinez-Vazquez[1]

Received: 24 August 2015 / Accepted: 17 October 2016 / Published online: 31 October 2016

Abstract This paper discusses the estimation of wind dynamic response of two types of structures by following classical and novel approaches. A new method for structural analysis based on wind design spectra is introduced and tested against simulated and experimental data. Design spectra are derived from the dynamic response of a group of oscillators subject to wind, using similar techniques than those used to derive design spectra for seismic engineering applications. The method is used on three chimneys of different height as well as on a regular building which has been experimentally tested in the past. The chimneys and building are also submitted to simulated wind fields to provide additional sets of results. It is observed that the spectral approach is consistent with experimental and simulated results and therefore is concluded that design spectra can cover broad range of practical applications.

Keywords Wind loading · Spectral analysis · Wind design spectra · CAARC benchmark building

Introduction

The most common methods to compute the dynamic response of structures subjected to wind include the gust load factor after Davenport (1967), load response correlation (Kapersky 1992), generalised gust factor (Piccardo and Solari 2000), gust response factor (Zhou and Kareem 1992), effective static load distribution (Holmes 2002), the equivalent static wind load (Chen and Kareem 2004; Chen and Zhou 2007) and the universal equivalent static load (Tamura and Katsumura 2012). These methods use load response correlation factors to obtain the mean and background dynamic response through a superposition of effects induced by equivalent (meaningful) static load configurations affected by peak factors. The structural dynamic response can also be obtained through numerical simulation techniques such as those described in Grigoriu (1998), Gurley and Kareem (1998), Deodatis and Micaletti (2001) and Rodriguez-Cuevas et al. (2006), amongst others. These techniques use theoretical wind spectra as argument of stochastic functions that generate partially correlated data series which once fed into a numerical integration procedure gives synthetic dynamic response histories.

The use of design spectra for modal analysis is normally applied in Seismic Engineering where it is assumed that inertial forces induced by the horizontal accelerations acting at base of the structure are fully correlated. The corresponding set of coupled equations of motion for a multiple degree of freedom lumped-mass system is solved through an uncoupled set of modal equations and the design spectra is then applied to compute the contribution of each mode of vibration to the total response, see for example Chopra (1995). In the case of wind loading, the forces distributed over the height of the structure are not fully correlated. However, the amount of energy imparted to the structural system can be estimated through suitable aerodynamic admittance functions to account for the lack of correlation of the wind gusts in relation to the size of the structure. The possibility of inferring wind response spectra using techniques that are analogous to those relevant to Seismic Engineering has been discussed in Solari (1989). That investigation showed that, however the

✉ P. Martinez-Vazquez
p.vazquez@bham.ac.uk

[1] School of Engineering, University of Birmingham, Birmingham B15 2TT, UK

contrast between the nature of wind and earthquake load, it is possible to conceive a consistent set of equations to determine scenarios of generalised wind loading that facilitate the determination of peak structural responses. Although the determination of design spectra, i.e. charts containing pseudo spectral accelerations associated to a range of frequencies or periods of vibration, is not actually realised in Solari (1989), these were visualised and the case was made. The present paper builds on such ideas and introduces a method to determine wind design spectra. This is done by assembling the dynamic response of a number of *sdof* oscillators with different mechanical and aerodynamical properties, not following the Equivalent Wind Spectrum Technique developed in Solari (1988, 1989) but maintaining cross-correlation functions similar to those proposed in Vickery (1970) and Tanaka and Lawen (1986a, b), to describe cross spectral properties of wind gusts. The dynamic responses generated in that way are resolved in the frequency domain by applying a transfer function to the input signal. The ensemble response accelerations expressed as function of the fundamental period of the oscillators then constitute a design spectrum. The spectral method is then tested a set of chimneys of different height as well as on the CAARC benchmark building whose structural response to wind load has been experimentally determined by a number of wind tunnel laboratories in the past (Melbourne 1980; Tanaka and Lawen 1986a, b). In the present study, the chimneys and building are also subjected to a simulated wind field to provide further insight into their dynamic performance. It is shown that the spectral approach is consistent with the simulation and available experimental results. The similarities and differences of the results obtained are subject of discussions throughout the paper.

The paper is organised in the following way: section two introduces the design spectra. In section three the simulation method is described. Sections four and five discuss the modelling and corresponding results of the case studies whilst some final remarks are provided in section six.

The design spectrum method

In considering a point-like structure the wind force spectrum given by Eq. (1) can be used to define a spectrum of input acceleration as in Eq. (2), i.e. the acceleration imparted by wind to the structural system. In these equations, $S_F\ (n)$ represents the force spectrum, n is the gust frequency, q is a force factor, m is the mass excited by the wind, and $S_u\ (n)$ is the wind power spectrum. The force factor is given by $q = ½\ \rho C_D\ A\ (1 + 2U)$—where C_D represents the drag coefficient, A ρ and U are the area exposed to wind, air density, and the average along-wind velocity component. The mathematical definition of the factor q is given in "Appendix".

$$S_F(n) = q^2 S_u(n) \tag{1}$$

$$S_A(n) = \left(\frac{q}{m}\right)^2 S_u(n) \tag{2}$$

$$H(n) = \frac{1}{K\sqrt{(1-r^2)^2 + 4\xi^2 r^2}} \tag{3}$$

$$J(n) = \frac{1}{\sqrt{(1-r^2)^2 + 4\xi^2 r^2}} \tag{4}$$

The transfer function for a single mass-spring system under dynamic equilibrium, i.e. $H\ (n) = \sigma_d\ (n)/F\ (n)$ (where $F\ (n)$, $_d\ (n)$ represent the acting force and standard deviation of displacement associated to the frequency n, respectively), is defined by Eq. (3)—see Gould and Abu-Sitta (1980). In this equation r represents the ratio n/n_0 where n_0 is the fundamental frequency of the structure, K represents the structural stiffness and ξ represents the fraction of critical damping defined as $\xi = c/4\ m\pi n_0$—being c the viscous damping. The transfer function $J\ (n) = m\sigma_a\ (n)/F\ (n)$ relating input to response acceleration of a single oscillator can be expressed as in Eq. (4) whereas the validity of this equation is demonstrated in Eq. (5).

$$\frac{F}{m} J(n) = 4\pi^2 n^2 \sigma_d(n), \tag{5a}$$

$$\frac{F}{\sigma_d(n)} J(n) = 4\pi^2 n^2 m = \frac{J(n)}{H(n)}, \tag{5b}$$

$$J(n) = KH(n). \tag{5c}$$

In Eq. (5a) the response acceleration is resolved on each harmonic of the domain $\sigma_d(n)$ whilst the input acceleration induced by the wind flow is represented by the term F/m. Figure 1 shows the shape of the function $J(n)$ for different levels of damping.

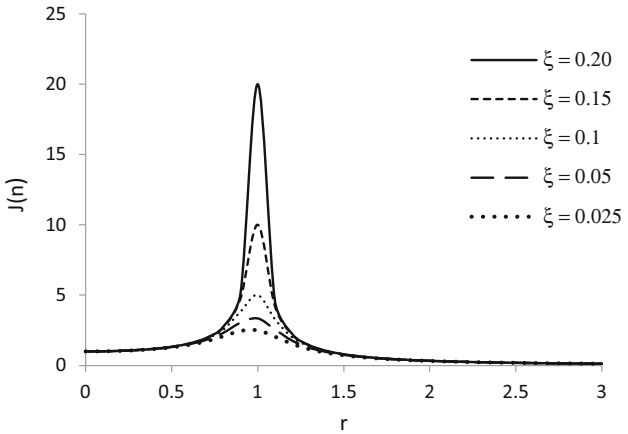

Fig. 1 Transfer function $J\ (n)$

The aerodynamic admittance as quoted in Dyrbye and Hansen (1997) is given in Eq. (6). That function accounts for the partial correlation of the wind field acting over the surface of the structure. The mean square response acceleration (σ_a^2) of a point-like structure can be estimated by combining Eqs. (2), (4) and (6), as in Eq. (7).

$$|X(n)| = \frac{1}{1 + \left(\frac{2n\sqrt{A}}{U}\right)^{4/3}}, \tag{6}$$

$$\sigma_a^2 = \int J^2(n) X^2(n) S_A(n) dn. \tag{7}$$

For *mdof* structures, Eq. (7) can be expressed in its generalised form in terms of the background and resonant components as in Eq. (8) and (9). In these equations, S_{cu} (n) and S_{Aij} (n) are the power spectral density of the generalised input acceleration and corresponding cross power spectrum. The cross power spectrum of input acceleration given in Eq. (8a) has been normalised by the square of the area of the structure (A) that is exposed to the wind, whereas ψ (z) accounts for the variation of turbulence with height. The horizontal and vertical distances between the points i, j located at coordinates $\{y_i, z_i\}$ and $\{y_j, z_j\}$ are denoted by Δ_y and Δ_z, respectively, $\Phi(z)$ stands for the modal ordinate at the height z and C_k represent the k-direction decay constant.

$$S_{A_{ij}}(z,n) = \frac{S_A(n)}{A^2} \psi(z) e^{-\frac{n_x}{U(z)}\sqrt{(C_y\Delta_y)^2 + (C_z\Delta_z)^2}}, \tag{8a}$$

$$S_{cu}(n) = \iint_A \phi(z_i)\phi(z_j) S_{A_{ij}}(z,n) \mathrm{d}y_i \mathrm{d}y_j \mathrm{d}z_i \mathrm{d}z_j, \tag{8b}$$

$$\sigma_{a,b}^2 = \int J^2(n) S_{\mathrm{cu}}(n) \mathrm{d}n, \tag{8c}$$

$$\sigma_{a,r}^2 = \frac{\pi n_0 S_{cu}(n_0)}{4\xi}. \tag{9}$$

The generalised formulation accepts $M^* = \int_0^H \Phi(z)^2 m \mathrm{d}z$ instead of m in Eq. (2). Figure 2 shows the spectrum of generalised input acceleration for a range of building dimensions determined by the width (W) and shape factor (S), and average velocity U, for a fraction of critical damping of 2.5%. In this case, W is the width of the area of the structure facing the wind flow, whereas S represents the ratio between the height of the structure and its width. The spectra shown in these figures were calculated by assuming a roughness length (z_0) of 0.3 m, turbulence intensity (I) of 0.295, gradient height (H_g) of 390 m, characteristic structural density (ρ_s) of 384 kg m^{-3}, damping (ξ) and aspect ratio (S) of 0.025 and 10, respectively.

It can be seen in Fig. 2 that the amount of energy input to the structure decreases at a slower rate along the frequency

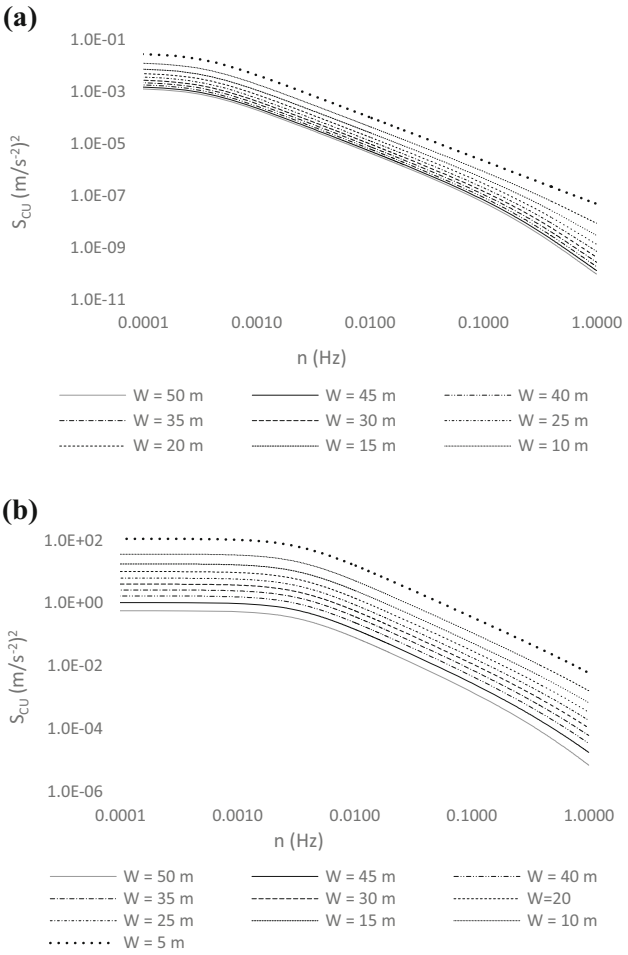

Fig. 2 Power spectral density of generalised input acceleration for **a** $U = 5$ ms^{-1}, **b** $U = 50$ ms^{-1}

axis as the wind speed increases. It is also evident that the decay of gusts' correlation with the distance (e.g. width) whereas for the range of wind speeds studied (5–50 ms^{-1}) the generalised input acceleration associated to gust components that occur at frequencies above 1 Hz is rather small. This seems consistent with the distribution of energy content that is reflected in the wind power spectrum.

In Eq. (8c) and Eq. (9), the terms $\sigma_{a,b}^2$ and $\sigma_{a,r}^2$ stand for the mean square background and resonant component of the response, respectively. The background component takes into account all frequencies of excitation excluding the resonant component (n_0)—noting that Eq. (8c) can be integrated over a range of frequencies $n < n_0$ by assuming that higher order frequencies will have a minimum contribution to the total response (Simiu and Scanlan 1996). It follows that the ensemble values of $\sigma_{a,b}$ and $\sigma_{a,r}$, i.e. the rms of Eq. (8) and (9), for a group of equivalent sdof systems with fundamental period (T_0) define the response spectra S_{a_b} (T_0) and S_{a_r} (T_0). Figures 3 and 4 show examples of response spectra for the background and

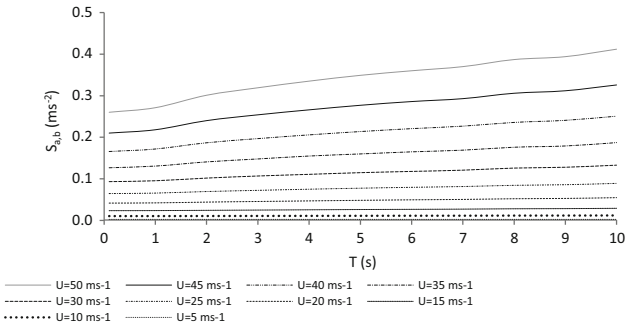

Fig. 3 Design spectra for $\xi = 0.025$, $S = 10$, and $W = 20$ m—background component

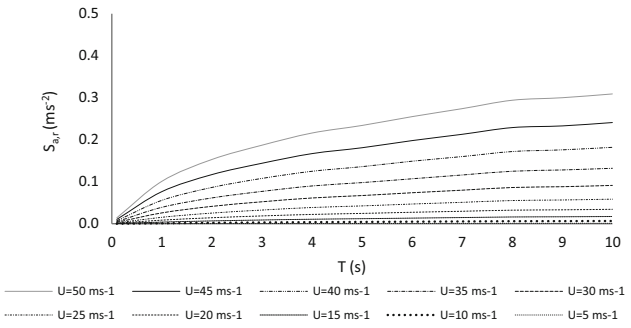

Fig. 4 Design spectra for $\xi = 0.025$, $S = 10$, and $W = 20$ m—resonant component

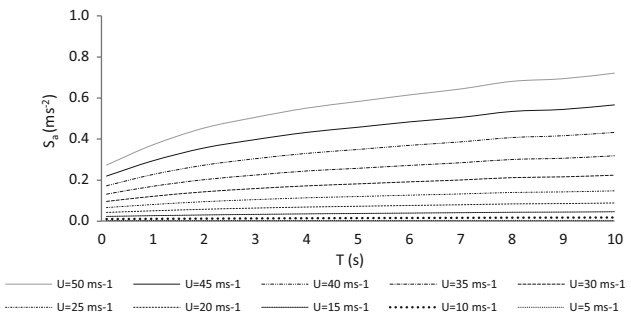

Fig. 5 Design spectra for $\xi = 0.025$, $S = 10$, and $W = 20$ m—total response

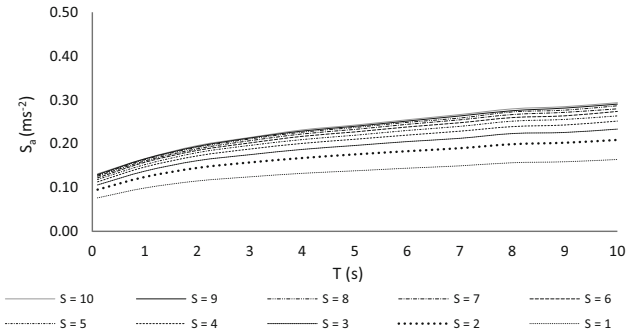

Fig. 6 Design spectra for $\xi = 0.025$, $U = 25$ ms^{-1}, and $W = 10$ m—total response

resonant contributions and their variation with the local average wind speed (U) calculated for the same wind and geometric conditions than the generalised input spectral acceleration shown in Fig. 2. Figure 5 shows the design spectrum which results from superimposing the values of S_{a_b} (T_0) and S_{a_r} (T_0) shown in Figs. 3 and 4.

Figures 3 and 4 show that the response acceleration increases with T_0, which would be the result of the gradual increase of the input acceleration as the fundamental frequency of the oscillator moves towards the low frequency range. It can also be seen that the resonant response component is more sensitive to the fundamental period of the oscillator than the background component. The ratio between $S_{a,r}$ ($T_0 = 10$ s; $n_0 = 0.1$ Hz) and $S_{a,r}$ ($T_0 = 1$ s; $n_0 = 1$ Hz) is of 7.05 and 3.06 when $U = 5$ and $U = 50$ ms^{-1}, respectively. This is about 6.5 and 2 times higher than the same parameter calculated for the background response component.

The influence of the aspect ratio *(S)* on the total response is shown on Fig. 6 whilst the effect of damping is presented in Fig. 7. Data in Fig. 6 correspond to an average wind velocity of 25 ms^{-1}, damping of 2.5%, and width of 10 m whilst data in Fig. 7 covers the particular case in which $S = 1$, $U = 15$ ms^{-1} and $W = 15$ m. The rest of parameters remained as before.

Figure 6 shows that the shape factor has an important impact on the design spectra. The increase of the ordinates of the response spectra for $S = 10$ with respect to $S = 1$ (this term referred to as S_{10}/S_1) is of about 63% for a reference period T_0 of 5 s. The impact of the shape factor to the response spectra has been found to be highly sensitive to U and W. For instance, by changing U whilst keeping constant W (10 m) ratio S_{10}/S_1 fluctuates between 40 and 80%. Conversely by changing W whilst keeping constant U (25 ms^{-1}), the ratio S_{10}/S_1 fluctuates between 70 and 250%. The little correlation found between damping and background response is also noticeable. The ratio between the ordinates of the background response for $T_0 = 10$ s and $T_0 = 0.1$ s is 1.26 for $\xi = 0.025$ and 1.03 for $\xi = 0.2$, whereas the equivalent measurement for the resonance component is $\sim$11.4 regardless of the damping level. Note that by varying the rest of controlling parameters, i.e. *U, S* and *W,* the ratio remains fairly constant for the background but not for the resonant response component. Based on this, it can be said that the resonant response is highly dependent on damping although the same cannot be said of the background component which is weakly correlated to that parameter—yet some dependence is predicted by Eq. (3). Therefore, the spectral variation with damping shown in Fig. 7 is basically caused by resonant effects.

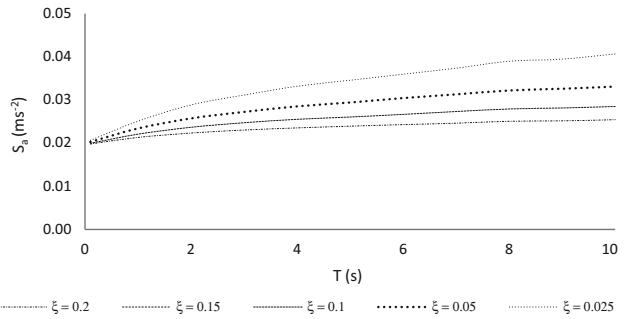

Fig. 7 Design spectra for $S = 1$, $U = 15$ ms^{-1}, and $W = 15$ m—total response

Simulated wind field

Synthetic wind fields to determine the instantaneous variation of structural displacements of the chimneys and building were produced. The time series analyses were used to compare results against those calculated through the spectral approach for all structures, and against experimental results in the case of the CAARC building. The wind field simulation is based on the algorithm suggested by Vanmarcke et al. (1993) which consists of inferring correlated data series in a number of target points across a region bounded by a number of stations in which the characteristics of the random signal are known. This process is based on the best estimator of Fourier coefficients that can be used to reconstruct power spectra at the target locations which are consistent with realistic correlation laws such as those described by Dyrbye and Hansen (1997) and Simiu and Scanlan (1996). The effectiveness of the method has been reported by a number of authors in the past, see for instance Gurley and Kareem (1998), Martinez-Vazquez and Rodriguez-Cuevas (2007a, b), Martinez-Vazquez and Sterling (2011). Therefore, a brief explanation of the method together with some statistics of simulation results is provided below.

The simulation consisted of generating two uncorrelated time series that represent the wind regime of a suburb at heights of 10 and 250 m above the ground, using Monte Carlo techniques. These time series were taken as recorded data in the algorithm discussed in Vanmarcke et al. (1993) from where partially correlated series at intermediate points could be inferred. The target turbulence intensity at $z = 10$ m was 0.295 and $\sim$0.2 for the towers and CAARC building, respectively. The former being a standard value for suburban area whilst the latter was the value used in the experimental work reported in Melbourne (1980) and in Tanaka and Lawen (1986a, b). Table 1 shows the statistics of the simulated series (case study 1: circular towers) located along the height of 250 for when the wind velocity at 10 m above the ground (U_{10}) is 33 ms^{-1}.

In Table 1, U and σ^2 represent mean and variance of the series in ms^{-1} and m^2 s^{-2} whereas the subscripts represent target *(t)* and simulated *(s)* values, respectively. The mean square error between target and simulated values are of 4.7% for the mean velocity and 0. 9% for the variance. The target and simulated cross-correlation amongst time series is shown in Tables 2 and 3.

The mean square error of the correlation parameter is of 1.135% across all stations. This was considered acceptable and representative of wind events in suburban areas. A comparison between the simulated and theoretical wind power spectrum in the low frequency range is shown in Fig. 8 for the position $z = 10$ m above the ground level.

The simulated power spectrum represents a single realisation and thus the spectral density fluctuates around the Von Karman spectrum. In Martinez-Vazquez and Rodriguez-Cuevas (2007a, b) and Martinez-Vazquez and Sterling (2011), it is demonstrated that, by increasing the number of realisations, the ensemble of simulated spectral ordinates tends to theoretical values. For the purpose of the present study, the single realisation of the synthetic fields are considered to be appropriate.

Case study 1: circular chimneys

Model description

The selected structures are three prismatic chimneys of 250, 150 and 75 m tall. These are fixed at the base and have walls of constant thickness. The material is steel with Young's modulus of 200 $\times$ 10^3 Nm^{-2}, Poisson's ratio of 0.3 and density of 7850 kg m^{-3}. The steel towers were modelled using computer software which enables time series and spectral analysis to be realised. The natural frequency analysis reports fundamental periods of vibration (T_0) of 4.21 s $(n_0 = 0.237$ Hz), 2.28 s $(n_0 = 0.439$ Hz), and 1.14 s $(n_0 = 0.875$ Hz) for the tower of $H = 250$ m, $H = 150$, m, and $H = 75$ m, respectively. These plus nine other frequencies are listed in Table 4 together with some geometrical properties of the towers such as diameter (D_t), walls thickness (t_w) and volumetric mass (m_v).

The design spectra presented in "The design spectrum method" section cover the interval of fundamental period of 0.1 s $\leq T_0 \leq$ 10 s which implies a cut off frequency of 10 Hz. Thus, for the analysis of the towers spectral ordinates up to until 100 Hz were estimated to account for at least vibrational 10 modes.

Dynamic response

The static forces induced by wind were calculated using Eq. (10). The reference height (z_r) was taken as of 10 m

Table 1 Calculated statistics of simulated wind time series

Stats\z (m)	10	40	75	100	140	170	200	210	220	240	250
U_t	32.24	45.25	51.41	55.36	58.79	61.39	63.90	64.70	65.36	66.43	67.14
U_s	32.98	45.23	51.38	55.34	58.76	61.37	63.83	64.65	65.31	66.38	67.09
σ_t^2	94.77	86.89	78.77	71.39	63.26	55.88	47.59	44.72	42.26	38.03	35.08
σ_s^2	94.82	86.94	78.81	71.43	63.30	55.91	47.78	44.83	42.36	38.18	35.22

Table 2 Target cross-correlation

	1	2	3	4	5	6	7	8	9	10	11
1	1.0000										
2	0.4237	1.0000									
3	0.2090	0.4767	1.0000								
4	0.1176	0.2605	0.5419	1.0000							
5	0.0653	0.1408	0.2895	0.5322	1.0000						
6	0.0394	0.0831	0.1690	0.3092	0.5798	1.0000					
7	0.0231	0.0479	0.0961	0.1748	0.3265	0.5625	1.0000				
8	0.0192	0.0394	0.0788	0.1429	0.2665	0.4588	0.8155	1.0000			
9	0.0164	0.0336	0.0669	0.1210	0.2255	0.3879	0.6893	0.8453	1.0000		
10	0.0127	0.0257	0.0508	0.0917	0.1705	0.2929	0.5200	0.6376	0.7543	1.0000	
11	0.0106	0.0213	0.0420	0.0756	0.1403	0.2408	0.4274	0.5240	0.6198	0.8217	1.0000

Table 3 Simulated cross-correlation

	1	2	3	4	5	6	7	8	9	10	11
1	1.0000										
2	0.4737	1.0000									
3	0.4100	0.6224	1.0000								
4	0.2255	0.3814	0.6510	1.0000							
5	0.2134	0.2928	0.5322	0.7333	1.0000						
6	−0.0052	0.1594	0.2694	0.4118	0.6122	1.0000					
7	−0.0591	0.0892	0.2860	0.4189	0.5377	0.5934	1.0000				
8	−0.1249	0.0231	0.2238	0.3157	0.4465	0.5431	0.8046	1.0000			
9	−0.1843	−0.0493	0.1078	0.2204	0.3681	0.5346	0.7388	0.8113	1.0000		
10	−0.1688	−0.0151	0.1387	0.2723	0.3842	0.4584	0.6270	0.6355	0.7276	1.0000	
11	−0.0237	0.0716	0.2322	0.2803	0.3309	0.3253	0.5227	0.5248	0.5858	0.7524	1.0000

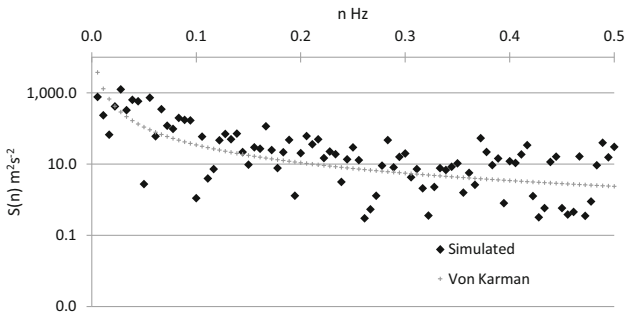

Fig. 8 Simulated and theoretical wind power spectrum at 10 m above the ground

whilst a value of $\alpha = 0.22$ was used to represent the wind profile in suburban area. Static forces and displacements calculated at the top of the structures (Δ_{top}) are given in Table 5.

$$F_i = \frac{1}{2}\rho C_D A_i U^2 \left(\frac{z}{z_r}\right)^{2\alpha}. \quad (10)$$

The displacements obtained through the time series and spectral analyses are presented in Table 6. These are the rms and peak dynamic response. In the context of the GLF, the peak dynamic response is expressed in terms of the mean (Δ) and rms (σ_r) response components as in

Table 4 Geometry and modal frequencies of the towers

H (m)	D_t (m)	t_w (m)	m_v kg m^{-3}	Mode									
				1	2	3	4	5	6	7	8	9	10
250	15	0.075	156	0.24	1.44	3.83	5.05	7.04	10.86	15.08	15.14	19.58	24.25
150	10	0.044	138	0.44	2.64	6.96	8.41	12.68	19.35	25.23	26.64	34.31	42.05
75	5	0.032	195	0.87	5.25	13.84	16.82	25.14	38.28	50.45	52.57	67.54	82.86

Table 5 Static forces (kN) and displacements

Tower/H (m)	10	40	75	100	140	170	200	250	Δ_{top} (m)
$H = 250$	255	614	817	919	1003	1130	1600	1055	0.94
$H = 150$	170	409	544	612	604	–	–	–	0.36
$H = 75$	85	204	148	–	–	–	–	–	0.11

Table 6 Dynamic displacements in (m) obtained through the time series and spectral analyses

Height/analysis	rms					
	$H = 250$ m		$H = 150$ m		$H = 75$ m	
	T-series	Spectral	T-series	Spectral	T-series	Spectral
0	0.0000	0.0000	0.0000	0.0000	0.0000	0.0000
10	0.0023	0.0023	0.0018	0.0021	0.0035	0.0022
25	0.0127	0.0126	0.0123	0.0140	0.0204	0.0139
40	0.0339	0.0332	0.0322	0.0361	0.0461	0.0336
60	0.0601	0.0584	0.0556	0.0618	0.0733	0.0539
75	0.0995	0.0960	0.0894	0.0984	0.1098	0.0807
90	0.1382	0.1325	0.1210	0.1323		
100	0.1815	0.1731	0.1546	0.1680		
122	0.2352	0.2230	0.1940	0.2103		
140	0.2894	0.2732	0.2316	0.2525		
150	0.3428	0.3224	0.2599	0.2844		
170	0.3981	0.3730				
185	0.4625	0.4315				
200	0.5280	0.4921				
225	0.6176	0.5781				
250	0.7152	0.6724				
Peak dynamic	2.53	2.43	0.96	1.02	0.42	0.34

Eq. (11)—see Davenport (1967), Zhou and Kareem (1992), Chen and Kareem (2004) and Chen and Zhou (2007).

$$R_{\max} = \Delta + g_r \sigma_r. \quad (11)$$

From the time series analysis, values of gust response factor (g_r) were inferred. These are 2.22, 2.31, and 2.82 for the towers of height $H = 250$ m, $H = 150$, m, and $H = 75$ m, respectively. This enabled to calculate the peak dynamic response values shown in Table 6.

The peak dynamic displacements shown in Table 6 correspond to the top of the structure. The spectral analysis deviates from the time series method as follows: ~4% (underestimate), 5.9% (overestimate), and ~20% (underestimate), for the tall, medium, and low-rise tower, respectively. The difference of displacement in the 75 m tall tower derives from the dynamic response. According to Table 6, the displacement at the top of the tower obtained via spectral method differs in about 0.029 m with respect to the time series analysis. The equivalent difference for the tall tower is 0.1 m, i.e. the two quantities representing a rate of variation ~0.04% along the height of the respective structure.

Case study 2: caarc building

Model description

The benchmark building was developed by the Common Wealth Advisory Aeronautical Research Council in 1969 (Melbourne 1980). Its primary purpose was the comparison of wind tunnel studies which could generate a reference point of standardisation in experimental modelling. The main characteristics of the building include plan dimension of 30.48 × 45.72 m and height of 183.88 m as shown in Fig. 9. The natural frequency of the model is 0.2 Hz along the v and w axes, the fraction of critical damping equals 0.01, and the volumetric mass is 160 kg m^{-3}.

In the year 1975, aeroelastic models of the CAARC building were experimentally tested in five different laboratories (Melbourne 1980; Tanaka and Lawen 1986a, b). The turbulence intensity used for the wind tunnels measured at the top of the building fluctuated around 0.1 whilst the same parameter measured at $z = 10$ m (full scale equivalent) was ~0.2. It was assumed that the power-law exponent of such boundary layer could be ~0.28—see Melbourne (1980), Tanaka and Lawen (1986a, b).

Dynamic response

Following the experimental work, the building's response is assumed to be totally based on the fundamental mode of vibration. The dynamic analysis was resolved using generalised properties of the building and numerical methods that are valid for *sdof* systems. The generalised force (F^*) and mass (M^*) were calculated with Eq. (12), where $\Upsilon(z)$ represents force or mass per unit length and ϕ is the fundamental modal shape which was approximated by $\phi(z) = (z/H)^{\beta}$—with $\beta = 1.5$. The generalised stiffness was obtained with $K^* = 4\pi^2 n_0^2 M^*$.

$$\Upsilon^* = \int_0^H \phi(z)^2 \Upsilon(z) \mathrm{d}z. \tag{12}$$

The static displacement was derived from the relationship $\Delta = F^*/K^*$ whereas the dynamic response was estimated via numerical integration of Eq. (14), which gives the solution to Eq. (13). The latter representing the dynamic equilibrium of one underdamped *sdof* oscillator subjected to random load. The numerical integration is done over each time step Δt where the initial and end forces, p_i and p_{i+1}, define the gradient s. The natural and damped frequencies are ω_n and ω_D, where $\omega_D = \omega_n\sqrt{1-\xi^2}$.

$$m\ddot{d} + c\dot{d} + kd = p(t) \tag{13}$$

$$d(t) = e^{-\xi\omega\Delta t}\left[\left(d(0) - \frac{p_i}{k} + \frac{2s\xi}{\omega_n k}\right)\cos(\omega_D \Delta t) + \left(\dot{d}(0) + d(0)\xi\omega_n - \frac{p_i\xi\omega_n}{k} + \frac{2s\xi^2}{k} - \frac{s}{k}\right)\frac{\sin(\omega_D\Delta t)}{\omega_D}\right] \times \frac{p_i}{k} + \frac{s\Delta t}{k} - \frac{2s\xi}{\omega_n k} \tag{14}$$

In addition to the static and numerical integration methods, the spectral analysis was completed using Eq. (15) to obtain the rms of displacement at the top of the building (σ_d). In this equation, L^* *and* M^* represent modal

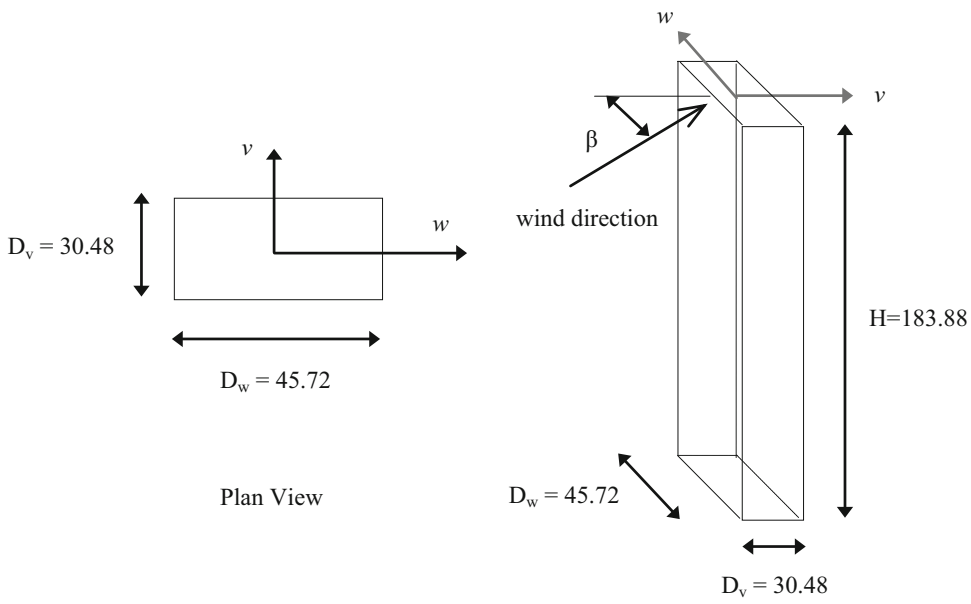

Fig. 9 Main characteristics of the CAARC benchmark building

excited masses and S_a is the spectral acceleration associated to the fundamental period (T_0).

$$\sigma_d = \phi \frac{L*}{M*} \frac{S_a}{\omega_n^2}, \tag{15a}$$

$$L^* = \int_0^H \phi(z) m(z) dz; \quad M^* = \int_0^H \phi(z)^2 m(z) dz. \tag{15b}$$

The spectral analysis was done for volumetric mass of 160 kg m^{-3} and wind velocities covering the range $5 \leq U_{10} \leq 25$ ms^{-1},i.e. similar range of velocities than the experimental tests presented in Melbourne (1980) and Tanaka and Lawen (1986a). Table 7 shows the spectral ordinates (S_a) associated to the natural frequency of the structure.

The spectral accelerations are different for the v and w directions since the value of generalised mass per unit height of the building depends on the width, e.g. the narrower the width of the building that faces the stream of wind the higher the mass per unit length that needs to be considered to work out the integration over the area as in Eq. (8).

The overall results of the static and dynamic analyses are shown in Table 8 where only displacements at the top of the building are presented. That is the only location at which experimental measurements were taken. The displacements corresponding to experimental tests (Exp.) shown in Table 8 were calculated with Eq. (16) below which is mapped from Melbourne (1980). In this equation, σ_k and D_k are the rms of displacement and width of the building for when the wind flows along the k-direction.

$$\frac{\Delta_v}{D_v} = 3.7 \times 10^{-4} \left(\frac{U_H}{n_0 D_w}\right)^2; \quad \frac{\sigma_v}{D_v} = 3 \times 10^{-5} \left(\frac{U_H}{n_0 D_w}\right)^3;$$
$$\frac{\Delta_w}{D_w} = 1.2 \times 10^{-4} \left(\frac{U_H}{n_0 D_w}\right)^2; \quad \frac{\sigma_w}{D_w} = 9.5 \times 10^{-6} \left(\frac{U_H}{n_0 D_w}\right)^3. \tag{16}$$

It can be seen in Table 8 that static displacements (Δ) calculated using the generalised approach are in good agreement with the experimental data. The dynamic (rms) response estimated via numerical integration and design spectra showed some larger variation when compared with experimental results. Although according to Melbourne (1980), Eq. (16) does not represent the best fit of experimental data in a mathematical sense and it does ignore the influence of some measurements that deviate from the rest, therefore it can only be used as a reference value. From this perspective it seems more convenient to compare the analytical results directly with experimental measurements as in Fig. 10.

Table 7 Spectral accelerations (ms^{-2}) calculated for the CAARC building

Wind direction	U_{10} (ms^{-1})				
	5	10	15	20	25
v	0.00537	0.0246	0.06075	0.1162	0.193
w	0.00363	0.01656	0.04087	0.0782	0.1293

The experimental data in Fig. 10 are reproduced from values published in Melbourne (1980). This figure shows that whilst fluctuations with respect to Eq. (16) occur, the results obtained through numerical integration and design spectra are consistent with the experimental measurements. This is demonstrated in Table 9 where the mean divergence with respect to Eq. (16) is presented for all sets of results.

In Table 9, it can be seen that static (analytical) displacements are very close to Eq. (16) in all cases. The displacements in the v-direction calculated with the spectral method vary less with respect to Eq. (16) than those provided by experimental testing from Western (The University of Western Ontario), NAE (a) (National Aeronautical Establishment in Canada), and Monash (Monash University in Australia). The difference when $U_{10} = 5$ ms^{-1} was found to be 0.0035 m, whilst for when $U_{10} = 25$ ms^{-1} the corresponding difference was of 0.0272 m. For the w-direction, the spectral approach deviates at a lower rate from Eq. (16) than the testing undertaken at Western, NAE (a) and NAE (b). In this case, the differences when $U_{10} = 5$ ms^{-1} was found to be of 0.0027 m, whilst when $U_{10} = 25$ ms^{-1} the difference was of 0.0238 m. The results from the numerical integration were compared to Eq. (16) as follows. The difference in the v-direction when $U_{10} = 5$ ms^{-1} was 0.0041 m and 0.0691 m when $U_{10} = 25$ ms^{-1}. For the w-direction, the differences were 0.0021 when $U_{10} = 5$ ms^{-1} and 0.0305 m when $U_{10} = 25$ ms^{-1}. According to this, the results obtained with the spectral approach provide closer results to the reference Eq. (16) than those calculated via numerical integration and in general these results fall within the range of accuracy observed in the experimental data.

Final discussion

The present investigation introduces design spectra to determine wind dynamic effects on regular prismatic structures and highlights the possibility of considering these in engineering practice. The rationale for the method is being drawn from previous research and seems compatible with simulation and experimental methods. It has been observed that background turbulence is weakly correlated with variations of spectral response along an axis representing natural vibration period (T_0) and therefore the variation of spectral ordinates with T_0 is mainly due to

Table 8 Static and dynamic displacements (m) at the top of the building

Wind direction	U_{10} (ms^{-1})	U_H (ms^{-1})	U_H n_0D_y	Static response		Dynamic response		
				$\Delta = F^*/K^*$	Exp.	Num. Int.	Spectral	Exp.
v	5	11.28	1.234	0.0171	0.0172	0.0058	0.0052	0.0017
	10	22.56	2.469	0.0685	0.0689	0.0233	0.0239	0.0138
	15	33.85	3.703	0.1541	0.1548	0.0526	0.0591	0.0465
	20	45.13	4.934	0.2740	0.2751	0.0934	0.1132	0.1101
	25	56.41	6.172	0.4281	0.4299	0.1460	0.1879	0.2151
w	5	11.28	1.234	0.0084	0.0084	0.0029	0.0035	0.0008
	10	22.56	2.469	0.0336	0.0334	0.0115	0.0161	0.0065
	15	33.85	3.703	0.0757	0.0752	0.0258	0.0398	0.0221
	20	45.13	4.934	0.1346	0.1337	0.0459	0.0761	0.0523
	25	56.41	6.172	0.2103	0.2089	0.0717	0.1259	0.1021

U_H wind velocity at the top of the building, n_0 fundamental frequency, D_y D_v or D_w

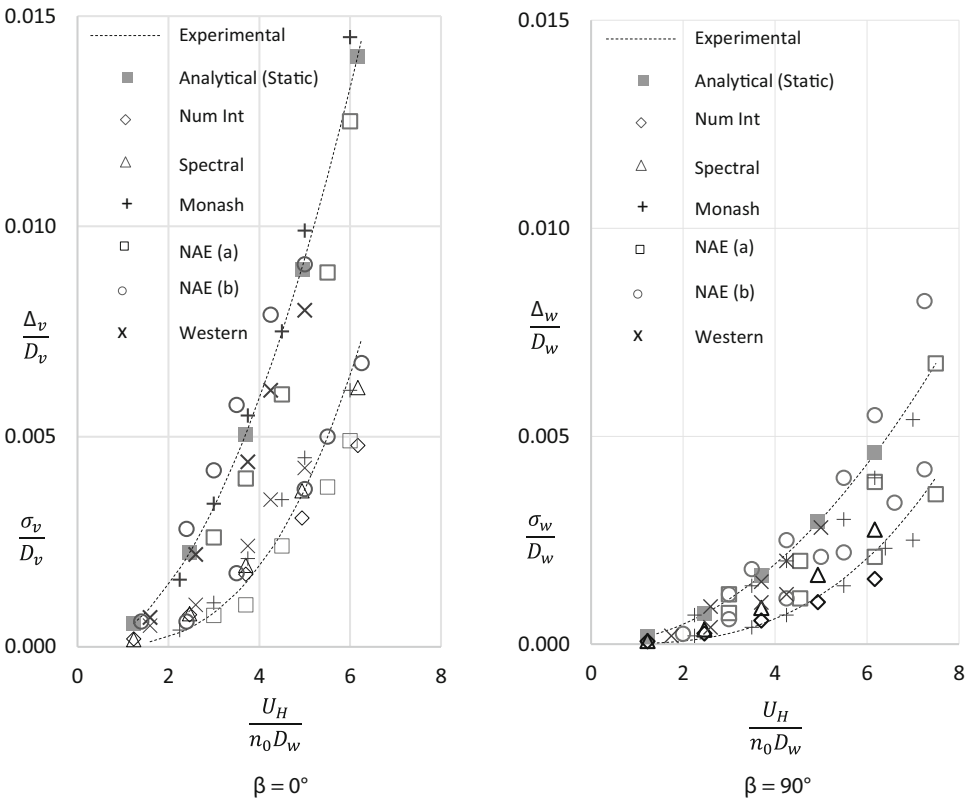

Fig. 10 Comparison of analytical results and experimental data discussed in Melbourne (1980)

Table 9 Mean divergence (m) of all methods with respect to Eq. (16)

Wind direction	Analysis	$\Delta = F^*/K^*$	Western	NAE (a)	NAE (b)	Monash	Num. Int.	Spectral
v	Static	0.0008	0.0194	0.0391	0.0216	0.0126		
	Dynamic		0.0205	0.0225	0.0075	0.0138	0.0211	0.0113
w	Static	0.0006	0.0069	0.0194	0.0321	0.0153		
	Dynamic		0.0157	0.0142	0.0210	0.0096	0.0095	0.0155

resonant effects. At the same time, it appears that damping does not have as much effect on the background response as it does on resonant effects, which to some extent can be predicted from the form of the transfer function that relates input to output acceleration. The spectral approach has been tested and compared against wind simulations and

experimental data from where it becomes evident that the idea of having a single set of true values for determining the structural response is impractical. However, the level of dispersion of results presented throughout the paper suggests that design spectra can be an alternative to existing methods for estimating the dynamic response of systems with various degrees of freedom.

Appendix

The total wind velocity is idealised as the superposition of mean (U) and fluctuating (u) wind velocity components as in Eq. (A1).

$$U_T = U + u. \tag{A1}$$

The total wind force can be expressed as in Eq. (A2), where C_D represents the drag coefficient, A is the area exposed to wind and ρ represents air density. The square of total wind velocity is given by Eq. (**A3**)

$$F = \frac{1}{2}\rho C_D A U_T^2, \tag{A2}$$

$$U_T^2 = (U+u)^2 = U^2 + 2Uu + u^2. \tag{A3}$$

The second and third term in Eq. (A3) represent the fluctuating wind velocity component which can be approximated as in Eq. (A4) to isolate the term u.

$$2Uu + u^2 \cong 2Uu + u = u(2U+1). \tag{A4}$$

Eq. (A4) can then be used for a spectral representation of the fluctuating wind loading. For instance,

$$S_F(n) = q^2 S_u(n), \tag{A5}$$

where

$$q = \frac{1}{2}\rho C_D A(2U+1).$$

References

Chen X, Kareem A (2004) Equivalent static wind loads on buildings: new Model. ASCE J Struct Eng 130(10):1425–1435

Chen X, Zhou N (2007) Equivalent static wind loads on low-rise buildings based on full-scale pressure measurements. Eng Struct. 29:2563–2575

Chopra A (1995) Dynamics of structures: theory and applications to earthquake engineering. Prentice Hall, Upper Saddle River

Davenport AG (1967) Gust loading factors. Am Soc Civil Eng J Paper 5255:11–34

Deodatis G, Micaletti RC (2001) Simulation of highly skewed non-gaussian stochastic processes. J Eng Mech 127(12):1284–1295

Dyrbye C, Hansen S (1997) Wind loads on structures. Wiley, Hoboken

Gould PL, Abu-Sitta S (1980) Dynamic response of structures to wind and earthquake loading. Pentech Press, London

Grigoriu M (1998) Simulation of stationary non-gaussian translation processes. J Eng Mech. 124(2):121–126

Gurley KR, Kareem A (1998) A conditional of normal velocity pressure fields. J Wind Eng Ind Aerodyn 77–78:39–51

Holmes JD (2002) Effective static load distribution in wind engineering. J Wind Eng Ind Aerodyn 90(2):91–109

Kapersky M (1992) Extreme wind load distributions for linear and non-linear design. Eng Struct 14(1):27–34

Martinez-Vazquez P, Rodriguez-Cuevas N (2007a) Wind field reproduction using neural networks and conditional simulation. Eng Struct 29(7):1442–1449

Martinez-Vazquez P, Rodriguez-Cuevas N (2007b) Dynamic response of A MDOF structure subjected to conditional simulation of wind time series. Publicaciones IIUNAM, Šid

Martinez-Vazquez P, Sterling M (2011) Predicting wheat lodging at large scales. Biosyst Eng 109:326–337

Melbourne WH (1980) Comparison of measurements on the CAARC standards tall building model in simulated model wind flows. J Wind Eng Ind Aerodyn 6:73–88

Piccardo G, Solari G (2000) Three dimensional wind excited response of slender structures: closed form solution. J Struct Eng 126(8):936–943

Rodriguez-Cuevas N, Martinez-Vazquez P, Marquez-Dominguez S (2006) Dynamic interaction between turbulent wind, and a slender tower. XV Mexican Congress in Structural Engineering (In Spanish)

Simiu E, Scanlan RH (1996) Wind effects on structures. Wiley, Hoboken

Solari G (1988) Equivalent wind spectrum technique. J Wind Eng Ind Aerodyn 114(6):1303–1323

Solari G (1989) Wind response spectrum. J Wind Eng Ind Aerodyn 115(9):2057–2073

Tamura Y, Katsumura A (2012) Universal equivalent static wind load for structures. The Seventh International Colloquium on Bluff Body Aerodynamics and Applications (BNAA7). Shanghai China, September 2–6

Tanaka H, Lawen N (1986) Test on the CAARC standard tall building model with a length scale of 1:1000. J Wind Eng Ind Aerodyn 25:15–29

Vanmarcke E, Heredia-Zavoni E, Fenton G (1993) Conditional simulation of spatially correlated ground motion. J Eng Mech. 119(11):2333–2352

Vickery BJ (1970) On the reliability of gust loading factors. Proceedings Technical Meeting concerning wind loads on buildings and structures. Build Sc Ser. 30. National Bureau of Standards, Washington D.C., p 93–104

Zhou Y, Kareem A (1992) Gust loading factor: new Model. J Struct Eng 127(2):168–175